CrystEngComm

Accepted Manuscript

ROYAL SOCIETY OF CHEMISTRY

www.rsc.org/crystengcomm

Six new coordination polymers based on a tritopic pyridyldicarboxylate ligand: Structures, Magnetic, and Sorption Properties

Tao Ding,[†,‡] Li-Di Ren,[‡] Xiao-Di Du,[‡] Li Quan,[‡] Zi-Wei Gao*[,†], Wei-Qiang Zhang,[†] Chang-Zheng Zheng*[,‡]

[†]*Key Laboratory of Applied Surface and Colloid Chemistry, Ministry of Education, School of Chemistry & Chemical Engineering, Shaanxi Normal University, Xi'an 710062, P. R. China.*

[‡]*College of Environment and Chemistry Engineering，Xi'an Polytechnic University，Xi'an 710048，P. R. China.*

E-mail: zwgao@snnu.edu.cn, (Z.-W. G); zgcgzg@126.com, (C.-Z. Z)

Using a rigid ligand, pyridine-3,5-bis(phenyl-4-carboxylic) acid (H_2L), six new coordination polymers have been synthesized under solvothermal conditions, formulated as [Co(L)(DMF)] (**1**), [Co(L)(H_2O)]·DMF (**2**), [$Co_3(L)_2(HCOO)_2(H_2O)_2$] (**3**), [$Co_5(L)_4(OH)_2(H_2O)_2$]·0.5DMF·$H_2O$ (**4**), [Mn(L)(H_2O)]·DMF (**5**), and [Zn(L)]·DMF (**6**) (DMF = N,N-Dimethylformamide). Complex **1** exhibits a 2D layer structure with four-connected net. **2** is also a 2D layer net which to from a 2D stacked layers porous framework through hydrogen bonding interactions. In **3**, 10-connected clusters [$Co_3(COO)_6$] are extended by L^{2-} linker to construct a 3D (3,10)-connected

framework with the $(4\cdot6\cdot8)(4^2\cdot6^2\cdot8^{10}\cdot10)$ topology net. As for **4**, a rare pentanuclear clusters $[Co_5(\mu_3\text{-}OH)_2(COO)_8N_4]$, which serves as a 12-connected node to give a 3D (3,12)-connected framework with a larger solvent accessible volume. **5** shows a 2D 4^4 layer framework by considering Mn(II) as a four-connected node. And **6** exhibits a 3D framework based on 1D Zn-(COO)-Zn chains. All complexes have been characterized by single-crystal X-ray diffraction, IR spectroscopy, elemental analysis, thermogravimetric analysis, and powder X-ray diffraction measurements. The magnetic properties of complexes **1**−**5** and the photoluminescence property for **6** have been investigated. H_2, N_2 and CO_2 adsorption measurements were carried out for **4**.

Introduction

The currently progressive impetus for the design and fabrication of novel coordination polymers (CPs) is due to not only their fascinating topology but also their promising properties and great potential applications in the fields of gas storage,[1] magnetism,[2] optical properties,[3] catalysis,[4] and so on. However, how to construct appropriate crystal structure is the primary issue, and many factors such as the organic ligand,[5] the coordination geometry of metals center,[6] and experimental conditions[7] can affect the final structures of CPs. Among all these factors, it has been observed that the organic ligand plays a crucial role for the design of some interesting coordination networks, such as the donating type, the flexibility, and the geometry of the organic ligands.[8] Among these various organic ligands, rigid aromatic multicarboxylates are the most effective ligands to bridge metal nodes into a variety of interesting open metal-organic

networks with various cavity dimensions and shapes for potential applications.[9] Usually, the polycarboxylate ligands with bent backbones, such as V-shaped, triangular, quadrangular, and so on,[10] are excellent candidates for building highly connected, interpenetrating, or helical coordination frameworks due to their bent backbones and versatile bridging fashions. Meanwhile, compared to the considerable research in the field of using carboxylate or pyridyl bridging ligands for building CPs, trifunctional pyridine-dicarboxylic acids which would act not only as a bridging carboxylate but also involve the terminal pyridyl N-donor which can afford extended and highly-connected framework.[11]

In this work, six new CPs based on a triangular ligand pyridine-3,5-bis(phenyl-4-carboxylic) acid (H_2L) have been synthesized, [Co(L)(DMF)] (**1**), $[Co(L)(H_2O)]\cdot DMF$ (**2**), $[Co_3(L)_2(HCOO)_2(H_2O)_2]$ (**3**), $[Co_5(L)_4(OH)_2(H_2O)_2]\cdot 0.5DMF\cdot H_2O$ (**4**), $[Mn(L)(H_2O)]\cdot DMF$ (**5**) and [Zn(L)]·DMF (**6**). All these complexes are characterized by single-crystal X-ray diffraction analyses. The structures and topological analyses of these complexes have been discussed in detail. In addition, the magnetic properties of **1**−**5**, the photoluminescence property of **6** and the H_2, N_2 and CO_2 adsorption for **4** have been studied.

Experimental

Materials and methods. Reagent grade H_2L ligand, $Co(NO_3)_2\cdot 6H_2O$, $MnCl_2\cdot 4H_2O$, $Zn(NO_3)_2\cdot 6H_2O$ and DMF. All solvent and starting materials for synthesis were purchased commercially and were used as received without further purification. Elemental analyses of C, H and N were performed on a Perkin-Elmer 240C analyzer.

IR spectra were measured on a FTIR-8400 spectrometer with KBr pellets. Thermal analysis was performed on a TGA/SDTA851 analyzer with a heating rate of 10 °C·min^{-1} under a N_2 atmosphere. Luminescence spectra for the solid samples were investigated with a Hitachi F-4500 fluorescence spectrophotometer. The X-ray powder diffraction pattern was recorded with a D/Max 3C diffractometer (λ = 1.5406 Å). Variable temperature magnetic measurements were carried out on a Quantum Design SQUID MPMS XL-7 instrument (2−300 K) in the magnetic field of 1 kOe. All the gas sorption isotherms were measured by using a ASAP 2020M adsorption equipment.

Synthesis of [Co(L)(DMF)] (1). A mixture of $Co(NO_3)_2·6H_2O$ (29.1 mg, 0.1 mmol), H_2L (31.9 mg, 0.1 mmol) and DMF(10 mL) was heated at 100 ºC for 72 h under autogenous pressure in a sealed 25mL Teflon-lined stainless steel vessel, and then cooled over a period of 24 h at a rate of 3 °C h^{-1}. Purple block crystals of **1** were collected by washing with DMF and dried in air. (Yield 53% based on H_2L). Anal. Calcd for $C_{22}H_{18}N_2O_5Co$: C, 58.81; H, 4.04; N, 6.23. Found: C, 58.63; H, 4.11; N, 6.17. IR(KBr, cm^{-1}): 3853(w), 3740(w), 3077(w), 2930(w), 1662(s), 1603(s), 1544(s), 1390(s), 1170(w), 1102(w), 1017(w), 859(m), 784(m), 707(w), 669(m), 536(w), 472(m).

Synthesis of [Co(L)(H_2O)]·DMF (2). 2 was synthesized by a solvothermal procedure similar to that described for **1** except using DMF (9 mL) and water (1 mL) instead of DMF (10 mL). Purple block crystals of **2** were collected by washing with DMF and dried in air. (Yield 61% based on H_2L). Anal. Calcd for $C_{22}H_{20}N_2O_6Co$: C,

56.54; H, 4.31; N, 5.99. Found: C, 56.36; H, 4.39; N, 5.85. IR(KBr, cm^{-1}): 3853(w), 3740(w), 3188(m), 2925(w), 1664(s), 1599(s), 1545(s), 1490(s), 1102(w), 1019(w), 859(m), 786(m), 670(m), 470(w).

Synthesis of $[Co_3(L)_2(HCOO)_2(H_2O)_2]$ (3). A mixture of $Co(NO_3)_2 \cdot 6H_2O$ (43.7 mg, 0.15 mmol), H_2L (47.9 mg, 0.15 mmol), DMF (3 mL) and water (7 mL) was heated at 130 ºC for 72 h under autogenous pressure in a sealed 25 mL Teflon-lined stainless steel vessel, and then cooled over a period of 30 h at a rate of 3 °C h^{-1}. Crimson block crystals of **3** were collected by washing with DMF and dried in air. (Yield 68% based on H_2L). Anal. Calcd for $C_{40}H_{28}N_2O_{14}Co_3$: C, 51.47; H, 2.59; N, 3.00. Found: C, 51.58; H, 2.65; N, 3.11. IR(KBr, cm^{-1}): 3222(w), 2830(w), 2360(m), 1609(s), 1410(s), 1188(w), 1012(w), 909(w), 864(m), 816(w), 774(m), 705(w), 674(w), 495(w), 444(w).

Synthesis of $[Co_5(L)_4(OH)_2(H_2O)_2] \cdot 0.5DMF \cdot H_2O$ (4). The same synthetic method as that for **1** was used except that DMF (10 mL) was replaced by DMF (8 mL) and water (2 mL). Pink block crystals of **4** were collected by washing with DMF and dried in air. (Yield 73% based on H_2L). Anal. Calcd for $C_{77.5}H_{55.5}N_{4.5}O_{21.5}Co_5$: C, 55.13; H, 3.31; N, 3.73. Found: C, 55.37; H, 4.24; N, 3.82. IR(KBr, cm^{-1}): 3749(w), 3193(m), 1606(s), 1541(s), 1395(s), 1184(w), 1011(w), 859(w), 782(m), 708(m), 668(w), 482(w).

Synthesis of $[Mn(L)(H_2O)] \cdot DMF$ (5). A mixture of $MnCl_2 \cdot 4H_2O$ (19.8 mg, 0.1 mmol), H_2L (31.9 mg, 0.1 mmol), DMF (9 mL) and water (1 mL) was heated at 80 °C for 72 h under autogenous pressure in a sealed 25 mL Teflon-lined stainless steel

vessel, and then cooled over a period of 20 h at a rate of 3 °C h^{-1}. Colorless block crystals of **5** were collected, washed with DMF and dried in air. (Yield 51% based on H_2L). Anal. Calcd for $C_{22}H_{20}N_2O_6Mn$: C, 57.03; H, 4.35; N, 6.05. Found: C, 57.29; H, 4.28; N, 6.16. IR (KBr, cm^{-1}): 3738(w), 3076(w), 2923(w), 1660(s), 1598(s), 1536(s), 1392(s), 1097(m), 1017(w), 860(m), 786(m), 706(m), 666(m), 467(m).

Synthesis of [Zn(L)]·DMF (6). A mixture of $Zn(NO_3)_2·6H_2O$ (29.7 mg, 0.1 mmol), H_2L (31.9 mg, 0.1 mmol), DMF (8.5 mL) and water (1.5 mL) was heated at 80 °C for 72 h under autogenous pressure in a sealed 25 mL Teflon-lined stainless steel vessel, and then cooled over a period of 20 h at a rate of 3 °C h^{-1}. Colorless block crystals of **6** were collected, washed with DMF and dried in air. (Yield 65% based on H_2L). Anal. Calcd for $C_{22}H_{18}N_2O_5Zn$: C, 57.97; H, 3.98; N, 6.15. Found: C, 57.73; H, 4.05; N, 6.08. IR (KBr, cm^{-1}): 3094(w), 2930(w), 1673(s), 1620(s), 1536(s), 1394(s), 1178(w), 1096(m), 1011(w), 856(w), 786(s), 706(m), 669(m), 564(w), 468(m).

Crystallographic Data Collection and Refinement. Single-crystal X-ray diffraction analyses of the four complexes were carried out on a Bruker SMART APEX-II CCD diffractometer, equipped with a graphite monochromator using Mo−Kα radiation (λ = 0.71073), by using a *Φ*/ω scan technique at room temperature. The structures were solved using direct methods and successive Fourier difference synthesis (SHELXS-97)[12a], and they were refined using the full-matrix least-squares method on F^2 with anisotropic thermal parameters for all non-hydrogen atoms (SHELXS-97)[12]. Hydrogen atoms of organic ligand were located at geometrically calculated positions and refined with isotropic thermal parameters. However, the OH^- hydrogen atoms of **4**

and water hydrogen atoms in **2**−**5** could not be theoretically generated, and they also have not been added by difference Fourier maps due to the lack of large enough Q peaks around the water oxygen atom. For complexes **2** and **6**, isolated DMF solvents within the channels were not crystallographically well-defined. The uncoordinated DMF molecules were determined on the basis of TGA and elemental analysis, and the data were treated with the SQUEEZE routine within PLATON.[12f] The crystallographic data and selected bond lengths and angles for **1**−**6** are listed in Table **1** and Table **S1**−**S6**.

(Insert Table **1** & **2**)

Results and discussion

Synthesis. The formation and/or crystallization of CPs are significantly influenced by the reaction temperature, solvent, metal cations, and so on.[7e,13] Reaction of the same initial reactants in different solvents or at different temperatures can generate diverse structures, which may provide direct evidence of the structural influence from these external factors. **1**, **2** and **4** were synthesized under the similar external experimental environment, the structural differences should mainly result from the different solubilities of $Co(NO_3)_2$ and H_2L in DMF and H_2O solvents. **4** was obtained at 100 °C, with the increase of solvent water, **3** was crystallized at a high temperature 130 °C. This may be due to the different boiling points of the solvent DMF and H_2O. **2**, **5** and **6** were synthesized under the similar reaction solvent and temperature except for the metal salts, the different products may be related to the different coordination environments of metal ions.

Structure of [Co(L)(DMF)] (1). As shown in Figure 1a, the structure of **1** contains one crystallographically unique Co(II) atom, one L^{2-} anion and one DMF molecule. Each Co(II) ion is six-coordinated by one nitrogen atom from one H_2L ligand [Co1−N1 = 2.139(4) Å], four carboxylate oxygen atoms from three L^{2-} anions [Co1−O = 2.033(4)−2.236(4) Å], and one DMF oxygen atom [Co(1)−O(5) = 2.191(5) Å] in an octahedral coordination geometry. All these bond lengths of Co–O/N match well with reported references.[14] Notably, carboxylate groups of L^{2-} anion exhibit two different coordination modes: one links one Co(II) atom in a chelating mode, while the other connects two Co(II) atom in a bridging mode. Subsequently, each H_2L ligand performs as a bridging/chelating ligand to join up two Co(II) atoms, which further propagate into a 2D 4^4 gridlike layer by the linkage of H_2L nitrogen atoms (Figure 1b). From a topological perspective, each Co(II) atom can be considered as 4-connected nodes, and L anion can be viewed as linker, so the structure of **1** can be best described as a 4^4 net (Figure 1c).

(Insert Figure 1)

Structure of [Co(L)(H_2O)]·DMF (2). As shown in Figure 2a, the structure of **2** is similar to **1**. It contains two crystallographically unique Co(II) atoms, two L^{2-} anion, two coordination water molecule and two lattice DMF molecule. The two Co(II) ions show similar coordination environment. Each Co(II) is six-coordinated by one nitrogen atom from one H_2L ligand, four carboxylate oxygen atoms from three L^{2-} anions and one water oxygen atom in an octahedral coordination geometry [Co−O bond distances are in the range of 2.032(19)− 2.253(2) Å, Zn−N bond distances are

2.158(2) and 2.162(2) Å]. Similarly to **1**, each H_2L ligand performs as a bridging/Chelating ligand to join up two Co(II) atoms, which further propagate into a 2D 4^4 gridlike layer by the linkage of H_2L nitrogen atoms (Figure 2b). Topological analysis of **2** shows that each metal ion acts as a four-connected node and L^{2-} anion can be viewed as linker to form a 4^4 sql net (Figure 2c).

(Insert Figure 2)

Structure of $[Co_3(L)_2(HCOO)_2(H_2O)_2]$ (3). The X-ray structure of **3** reveals that the asymmetric unit consists of one and a half Co(II) ion, one L^{2-} anion, one $HCOO^-$ anion and one coordination water molecule. The $HCOO^-$ anion is generated in situ by the hydrolysis of DMF molecules under solvothermal conditions[15]. Each Co1 exhibits distorted octahedral geometry with three oxygen atoms from two L^{2-} anions, one N atom from L^{2-} anion, one oxygen atom from $HCOO^-$ anion, and one oxygen atom from the water molecule. The Co2 ion is also six-coordinated by four O atoms from four L^{2-} anion, two oxygen atoms from two $HCOO^-$ anions [Co−O bond distances are in the range of 2.030(14)−2.216(13) Å, Co−N bond distance is 2.094(13) Å]. One Co2 and two Co1 ions are bridged by six carboxylate groups to form a linear $Co_3(CO_2)_6$ trinuclear cluster (Figure 3a).

The crystal of structure **3** exhibits a 3D network (Figure 3b) composed of trinuclear $Co_3(COO)_6$ cluster and L^{2-} bridging ligand. Each trinuclear cluster $Co_3(COO)_6$ acts as a node and is linked to ten nearby cluster by L^{2-} bridges (Figure 3c). Therefore, the cluster acts as a 10-connecting node in the overall structure. The L^{2-} anions act as 3-connecting nodes coordinating to three clusters in turn. The overall framework of **3**

can be described as a binodal (3,10)-connected network with the $(4\cdot6\cdot8)(4^2\cdot6^2\cdot8^{10}\cdot10)$ Schläfli symbol (Figure 3d).

(Insert Figure 3)

Structure of $[Co_5(L)_4(OH)_2(H_2O)_2]\cdot0.5DMF\cdot H_2O$ (4). The crystal structure of **4** exhibits a 3D network composed of pentanuclear $[Co_5(\mu_3\text{-}OH)_2(COO)_8]$ cluster nodes and L^{2-} bridging ligands. There are five crystallographic independent Co(II) atoms in **4** (Figure 4a). Co1 is six-coordinated with a distorted octahedral geometry with three oxygen atoms from three L^{2-} anions, one oxygen atoms from one water molecule and one oxygen atoms from one hydroxyl group. Both Co2 and Co3 adopt a distorted octahedral coordination geometry with one nitrogen atom from one L^{2-} anion, four oxygen atom from four L^{2-} anion and one oxygen atom from one hydroxyl group. Co4 and Co5 also adopt a distorted octahedral coordination environment and is coordinated by one nitrogen atom from one L^{2-} anion, three oxygen atoms from three L^{2-} anions, one oxygen atom from one water molecule and one oxygen atoms from one hydroxyl group [Co−O bond distances are in the range of 2.020(4)−2.277(4) Å, Co−N bond distances are in the range of 2.155(5)−2.224(5) Å]. The Co···Co distances bridged by the μ_3-hydroxyl group are 3.184, 3.407, 3.700, 3.534, 3.543, and 3.426 Å, respectively.

As mentioned above, there are pentanuclear $[Co_5(\mu_3\text{-}OH)_2(COO)_8]$ clusters which act as nodes in the overall 3D network (Figure 4b). Each cluster is supported by eight carboxylate groups that also bridge between Co(II) atoms. Furthermore, there are four nitrogen atoms from L^{2-} anions and two oxygen atoms from water molecules

also coordinated to the cluster and one water oxygen atom coordinate in bidentate fashion. All these carboxylate and nitrogen atoms bridge to adjoining clusters. Each pentanuclear cluster $[Co_5(\mu_3\text{-}OH)_2(COO)_8]$ acts as a node and is linked to twelve nearby clusters by L^{2-} bridges (Figure 4c). Therefore, the cluster acts as a 12-connecting node in the overall structure. In turn, the L^{2-} anions act as 3-connecting nodes coordinating to three clusters. The overall framework of **4** can be described as a binodal (3,12)-connected network with the $(4^{15}\cdot6^{36}\cdot8^{15})(4^2\cdot6)(4^2\cdot6)(4^3)(4^3)$ Schläfli symbol (Figure 4d). The channels in **4** are filled with guest DMF and water molecules. The effective free volume of **4** was calculated by PLATON analysis as 49.0% of the crystal volume (5998.7 $Å^3$ out of the 12230.0 $Å^3$ unit cell volume). The overall framework of 4 is a rare (3,12)-connected 3D porous network (Figure 4e), which can be desolvated to afford porous materials that can absorb H_2, N_2 and CO_2.

(Insert Figure 4)

Structure of [Mn(L)(H_2O)·DMF] (5). 5 crystallizes in triclinic space group *P*-1 and its asymmetric unit contains one Mn(II) atom, one L^{2-} anion, one coordinated water molecule and one lattice DMF molecule. The Mn(II) center is six-coordinated by four carboxylic oxygen atoms from three L^{2-} anions [Mn1−O bond distances are in the range of 2.121(2)−2.291(2) Å], one nitrogen atom from the L^{2-} anion [Mn1−N1 = 2.317(3) Å], and one oxygen atom from coordinated water molecule [Mn1−O1W = 2.201(3) Å], showing a distorted coordination octahedral geometry (Figure 5a). All these bond lengths of Mn-O/N fall in the usual range for similar compounds.[16] Subsequently, each H_2L ligand performs as a bridging ligand to join up two adjacent

Mn(II) atoms with the Mn···Mn separation of 4.26 Å, which further propagate into a 2D 4^4 gridlike layer by the linkage of nitrogen atoms from L^{2-} anions (Figure 5b). Further, the 2D layers arrange in an offset way with the grid of each layer occupied by groups from the adjacent ones (Figure 5c).

(Insert Figure 5)

Structure of [Zn(L)·DMF] (6). 6 crystallizes in monoclinic space group *C2/c*. The asymmetric unit of **6** is made up of one unique Zn(II) atom, one L^{2-} anion, and one lattice DMF molecule. Each Zn(II) atom coordinates to four oxygen atoms from four L^{2-} anions in the equator plane [Zn−O1 = 2.310(3), Zn−O2 = 1.965(2) Å], and one nitrogen atom of a L^{2-} anion in the axial position [Zn−N = 2.067(4) Å], showing a distorted square-pyramidal coordination environment (Figure 6a). Both Zn−O and Zn−N bond lengths are well-matched to those observed in similar complexes.[17] Two adjacent Zn(II) atoms are bridged by carboxylate groups with the Zn···Zn distance of 4.245 Å. The bimetallic Zn(II) units are linked by the carboxylate groups in the same way to form a $[Zn_2L_2]_n$ DNA-like chain along b axis (Figure 6b). Then, such chains are further linked by the L^{2-} anions to furnish a dimer-based layer, as illustrated in Figure 6c. Moreover, these 2D layers are further extended by the connection of a Zn-N bond to give birth to a 3D framework (Figure 6d).

(Insert Figure 6)

PXRD and TGA Analysis. PXRD has been used to check the phase purity of the bulk samples in the solid state. As shown in Figure S1 in the Supporting Information, the measured XRPD patterns of **1**–**6** are in good agreement with the ones simulated

from their respective single-crystal X-ray data, which clearly indicate the good purity and homogeneity of the synthesized samples. To identify the thermal stabilities of these complexes, the TGA measurements were carried out. TG curves for complexes **1**−**6** are shown in Figure S2, Supporting Information. For complex **1**, the first weight loss of 14.68% (calcd 16.25%) is observed from 174 to 241 ºC corresponds to the release of one coordinated DMF molecule. The removal of the organic components occurs in the range of 426−606 ºC. The remaining weight is assigned to Co_2O_3 (obsd, 18.51%; calcd, 18.46%). For complex **2**, a small weight loss of 3.81% (calcd 3.84%) is observed from 66 to 94℃ due to the release of one coordinated water molecule. The following weight loss from 162 to 223 ºC (obsd, 15.04%; calcd, 15.55%). Similarly to complex **1**, the removal of the organic components occurs in the range of 427−604 ºC. The remaining weight is assigned to Co_2O_3 (obsd, 17.79%; calcd, 17.67%). The first loss in complex **3** occurs in the range 158−193 ºC, implying removal of one coordinated water molecules (obsd 3.75%, calcd 3.82%). Then the TGA trace for **3** shows a gradual weight loss of 9.45% (calcd 9.56%) from 276 to 396℃, corresponding to the release of one coordinated $HCOO^-$ anions. The removal of the L^{2-} occurs in the range of 401-628 ºC. The remaining weight is attributed to the formation of Co_2O_3 (obsd, 28.26%; calcd, 26.54%). For complex **4**, the first loss of 7.28% (calcd 7.15%) in the temperature range of 45−227 ºC can be assigned to the release of lattice water and DMF molecules, coordinated water molecules, and hydroxyl groups. The decomposition of the residual composition begins from 385 to 601 ºC. Co_2O_3 was formed as the remaining residue (obsd, 24.16%; calcd, 23.81%).

The first weight loss in complex **5** occurs in the range 71−189 ºC, implying removal of the free DMF molecule (obsd, 18.19%; calcd, 15.76%), leaving a framework of [Mn(L)(H_2O)]. And then the framework begins to decompose at 437 ºC. Finally the residue is MnO (obsd 16.85%, calcd 15.31%). The TG curve for **6** shows the initial weight loss in the temperature range of 87−191 °C corresponds to the removal of free DMF molecule (obsd, 15.13%; calcd, 16.02%). Further weight loss observed from 438 °C indicates the decomposition of coordination framework. According to the above TGA of the six CPs, the solvent-free composition of these complexes begin to decompose beyond 380 °C; especially the frameworks of **1**, **2**, **5** and **6** collapsed from 426 °C, respectively, which indicated the higher thermal stability of these four complexes than others.

Magnetic Property. The temperature-dependent magnetic susceptibilities were measured on powdered samples of **1−5** at 1000 Oe in the range of 1.8-300K. The $\chi_M T$ and χ_M versus T plots of **1−5** are shown in Figure 7. For **1**, the $\chi_M T$ value of each Co_2 dimer at 300 K is 3.00 cm^3 mol^{-1} K, indicating the orbital contribution arising from the high-spin octahedral Co(II). It is well-known that the Co(II) in an octahedron possesses a $^4T_{1g}$ ground state, and thus the orbit angular momentum of the Co(II) ion will have a large contribution to the magnetic susceptibilities of these complexes. Upon cooling, $\chi_M T$ decreases monotonously to achieve a minimum value of 0.75 cm^3 mol^{-1} K at 1.8 K, suggesting an appreciable antiferromagnetic exchange between the between the magnetic centers in Co_2 dimer. The antiferromagnetic interaction may be considered to occur between Co_2 dimer bridged by carboxylic groups, whereas the

exchange interactions between Co(II) ions bridged through the nitrogen atom from L^{2-} anion can be ignored because of the long Co···Co separations[18]. Above 20 K, the temperature dependence of $1/\chi_M$ obeys the Curie-Weiss law with C = 3.13 cm^3 K mol^{-1} and θ = -13.8 K (see Figure 7a, insert), revealing dominant antiferromagnetic interactions between the Co_2 dimer and the presence of spin-orbit couplings.

As shown in Figure 7b, the $\chi_M T$ value of **2** are 5.79 cm^3 mol^{-1} K at 300 K, which is larger than the value for two magnetically isolated spin-only S = 3/2 Co^{2+} systems (3.75 cm^3 mol^{-1} K), indicating the important orbital contribution arising from the high-spin octahedral Co(II). Upon cooling, $\chi_M T$ decreases smoothly to reach a minimum value of 1.87 cm^3 mol^{-1} K at 1.8 K, suggesting a significantly antiferromagnetic exchange between the Co(II) ions connected through two O-C-O bridges. The $\chi_M T$ value (4.06 cm^3 mol^{-1} K) of **2** at the room temperature is larger than that of **1** (3.00 cm^3 mol^{-1} K, 2.03 cm^3 mol^{-1} K), which is possibly because the distance of two Co(II) ions bridged by carboxylic groups of **2** (4.427 Å) is shorter than that of **1** (4.531 Å). The short Co···Co distance is mainly responsible for the antiferromagnetic property of **2**. Above 30 K, the temperature dependence of $1/\chi_M$ obeys the Curie-Weiss law with C = 6.07 cm^3 K mol^{-1} and θ = -14.06 K (see Figure 7b, insert), indicating dominant antiferromagnetic interactions between the Co(II) ions and the presence of spin-orbit couplings.

The $\chi_M T$ and χ_M versus T plots of **3** are shown in Figure 7c. The $\chi_M T$ value at 300 K is 9.29 cm^3 mol^{-1} K, which is larger than the calculated spin-only value (5.625 cm^3 mol^{-1} K) for three Co(II) (S = 3/2) ions, indicating the orbital contribution arising

from the high-spin octahedral Co(II). Upon cooling, $\chi_M T$ first decreases smoothly to reach a minimum value of 6.72 $cm^3 mol^{-1} K$ at 10 K, then increases rapidly to a maximum of 8.05 $cm^3 mol^{-1} K$ at 1.8 K. This observation of a minimum is as expected for a ferromagnetic-like behavior.[19] Above 30 K, the temperature dependence of $1/\chi_M$ obeys the Curie-Weiss law with C = 9.71 $cm^3 K mol^{-1}$ and θ = -13.8 K (see Figure 7c, insert), indicating dominant antiferromagnetic interactions between the Co(II) ions and the presence of spin-orbit coupling. The antiferromagnetic exchange may be considered to occur between the Co(II) ions connected to each other through μ_2-O and O-C-O bridges. The big Co1-O1-Co2 angle of 105.87° and the short Co···Co distance of 3.440 Å are responsible for the strong antiferromagnetic interaction.

For **4**, as shown in Figure 7d, The $\chi_M T$ value at 300 K is 11.39 $cm^3 mol^{-1} K$, which is larger than the calculated spin-only value (9.375 $cm^3 mol^{-1} K$) for five Co(II) (S = 3/2) ions, indicating the orbital contribution arising from the high-spin octahedral Co(II). Upon cooling, $\chi_M T$ decreases monotonously to achieve a minimum value of 2.2 $cm^3 mol^{-1} K$ at 1.9 K, suggesting an appreciable antiferromagnetic exchange between the Co(II) ions connected through two μ_3−O and O−C−O bridges. The Co1-O(1W)-Co3, Co1-O(1W)-Co4, Co3-O(1W)-Co4, Co1-O(3W)-Co2, Co1-O(3W)-Co5, and Co2-O(3W)-Co5 angles are 130.16(18)°, 102.22(16)°, 113.67(17)°, 117.52(17)°, 117.53(17)°, and 111.32(16)°, respectively. These large Co−O−Co angles are generally indications of antiferromagnetic interactions. Above 20 K, the temperature dependence of $1/\chi_M$ obeys the Curie−Weiss law with C =13.45 $cm^3 K mol^{-1}$ and θ = -51.69 K (see Figure 7d, insert), revealing dominant antiferromagnetic interactions

between the Co(II) ions and the presence of spin−orbit couplings.

The $\chi_M T$ and χ_M versus T plots of complex **5** are shown in Figure 7e. The $\chi_M T$ value per Mn(II) for **5** at 300 K is about 4.71 $cm^3 mol^{-1} K$, higher than the spin-only value (4.38 $cm^3 mol^{-1} K$) expected for an uncoupled high-spin Mn(II) ion. As the sample is cooled, the $\chi_M T$ value decreases continuously, while the χ_M value increases to a broad maximum at about 8 K, then decreases on further cooling. The data above 20 K follow the Curie–Weiss law with C = 4.91 $cm^3 K mol^{-1}$ and θ = -12.76 K (see Figure 7e, insert), indicating antiferromagnetic interactions between the neighboring Mn(II) centers.

According to the structures of **5**, it could be presumed that the main magnetic interactions between the metal centers might happen between two bridged Mn(II) ions through O-C-O bridges, whereas the superchange interactions between Mn(II) ions through the nitrogen atoms and another carboxylate groups from L^{2-} anions can be ignored because of the long length of L^{2-} ligands. Thus, the system of **5** can be regarded as isolated Mn(II) groups from the magnetic viewpoints, despite the 2D structural feature.

Adsorption Studies. In order to assess the porosity of **4**, the N_2 and CO_2 sorption isotherms were performed at 77 and 195 K, which display type-I isotherms and the maximum N_2 and CO_2 uptakes are 51.9 and 105.2 $cm^3 g^{-1}$, respectively (Figure 8a). The hysteresis curves should arise from the hindered escape of adsorbed gases in the pores during the desorption process for the kinetic diameters of N_2 (3.64 Å) and CO_2 (3.30 Å) are close to the pore sizes of **4**, therefore, it shows a more obvious hysteresis

for N_2 desorption due to its larger kinetic diameters. The Brunauer−Emmett−Teller (BET) and Langmuir surface areas of 141 and 187 $m^2 g^{-1}$, as well as a median pore width of 5.5 Å is available by applying the Horvath-Kawazoe method. Furthermore, we further studied its storage capacity for the attractive energy carrier gas hydrogen. The hydrogen gas adsorption isotherms measured at 77 K and 1 atm. **4** adsorbs 108.65 $cm^3 g^{-1}$ (0.97 wt%) H_2 (Figure 8b), which is relatively high for pores MOFs, such as the best zeolite ZSM-5 (0.7 wt%).[20] For **4**, the significant CO_2 and H_2 sorption selectivity over N_2 may be attributed to the smaller kinetic diameters of CO_2 and H_2 than that of N_2 (H_2, 2.80 Å). The selective sorption of CO_2 rather than N_2 gas can also be attributed to the significant quadrupole moment of CO_2 (4.30×10^{-26} esu^{-1} cm^{-1}) compared to N_2 (1.52×10^{-26} esu^{-1} cm^{-1}). In the structure of **4**, the numerous coordinated −OH donors and pyridine groups of L^{2-} on the pore walls can interact effectively with quadrupole molecules, which can generate strong interactions with the host framework.[21]

Luminescent Properties. The coordination polymers with d^{10} metal centers have been investigated for fluorescence properties with potential applications in photochemistry, chemical sensors, and light-emitting diodes.[22] The photoluminescence spectra of complex **6** and the free ligand H_2L were examined in the solid state at room temperature (Figure 9). The free H_2L ligand exhibits a weak emission at 357 nm when excited at 275 nm, which can be assigned to the ligand-centered electronic transitions, that is, the $\pi^* \rightarrow n$ or $\pi^* \rightarrow \pi$ electronic transitions.[23] As shown in Figure **9**, the main emission peaks of complex 6 were

observed at 363 nm (λ_{ex} = 275 nm). Because the Zn(II) ions are difficult to oxidize or to reduce, the emission of **6** is neither metal-to-ligand charge transfer (MLCT) nor ligand-to-metal charge transfer (LMCT) in nature.[24] As a result, the emission of **6** can be assigned to intraligand transitions.[25] Although more detailed theoretical and spectroscopic studies may be necessary for better understanding of the luminescent mechanism, the strong fluorescence emissions of those d^{10} CPs make them potentially useful photoactive materials.

Conclusions

In summary, six new CPs based on rigid pyridine-3,5-bis(phenyl-4-carboxylic) acid ligand have been synthesized. Assemblies of these complexes generate diverse types of framework. Complex **1, 2** and **5** exhibit 2D layer networks. Three 3D frameworks with a (3,10)-connected network for **3**, a (3,12)-connected network with microporous network for **4** and 3D framework based on 1D chains for **6** are observed. Magnetic studies reveal that complex **1**, **2**, **4** and **5** show antiferromagnetic exchanges between metal ions, while dominant antiferromagnetic interactions (in 300−30 K) and ferromagnetic-like behavior (at low temperature) are observed in **3**. In addition, complex **4** exhibits microporous sorption for N_2, H_2 and CO_2 and **6** shows good photoluminescence property.

Supporting Information

Electronic Supplementary Information (ESI) available: Crystallographic information files (CIF), PXRD, and TGA. See DOI: 10.1039/b000000x/

Acknowledgements

This work was supported by the 111 Project (B14041), Innovative Research Team in University of China (IRT1070), the National Natural Science Foundation of China (21271124, 21371112), the Fundamental Research Funds for the Central Universities (GK201302015, GK201002031), Doctoral Fund of Ministry of Education of China (20120202120005) and Natural Science Basic Research Plan in Shaanxi Province of China (2012JM2006).

Notes and references

(1) (*a*) U. Mueller, M. Schubert, F. Teich, H. Puetter, K. Schierle-Arndt, J. Pastre, *J. Mater. Chem.*, 2006, **16**, 626; (*b*) M. Dincă, A. Dailly, Y. Liu, C. M. Brown, D. A. Neumann, J. R. Long, *J. Am. Chem. Soc.*, 2006, **128**, 16876; (*c*) S.-Q. Ma, D.-F. Sun, X.-S. Wang, H.-C. Zhou, *Angew. Chem., Int. Ed.*, 2007, **46**, 2458; (*d*) J. L. C. Rowsell, O. M. Yaghi, *Angew. Chem. Int. Ed.*, 2005, **44**, 4670.

(2) (*a*) O. Sato, Acc. *Chem. Res.*, 2003, **36**, 692; (*b*) E.-Q. Gao, Y.-F. Yue, S.-Q. Bai, Z. He, C.-H. Yan, *J. Am. Chem. Soc.*, 2004, **126**, 1419; (*c*) X.-Y. Wang, Z.-M. Wang, S. Gao, *Chem. Commun.*, 2008, 281; (*d*) X.-N. Cheng, W.-X. Zhang, Y.-Y. Lin, Y.-Z. Zheng, X.-M. Chen, *Adv. Mater.*, 2007, **19**, 1494.

(3) (*a*) E. Cariati, M. Pizzotti, D. Roberto, F. Tessore, R. Ugo, *Coord. Chem. Rev.*, 2006, **250**, 1201; (*b*) O. R. Evans, W. B. Lin, *Chem. Mater.*, 2001, **13**, 2705.

(4) (*a*) J. Y. Lee, O. K. Farha, J. Roberts, K. A. Scheidt, S. T. Nguyen, J. T. Hupp, *Chem. Soc. Rev.*, 2009, **38**, 1450; (*b*) J. S. Seo, D. Whang, H. Lee, S. I. Jun, J. Oh, Y. J. Jeon, K. Kim, *Nature*, 2000, **404**, 982; (*c*) R.-Q. Zou, H. Sakurai, Q. Xu,

Angew. Chem. Int. Ed., 2006, **45**, 2542; (*d*) C. Dey, R. Das, B. K. Saha, P. Poddar, R. Banerjee, *Chem. Commun.*, 2011, **47**, 11008.

(5) (*a*) Y. -F. Hsu, H. -L. Hu, C. -J. Wu, C. -W. Yeh, D. M. Proserpio, J. -D. Chen, *CrystEngComm*, 2009, **11**, 168; (*b*) D. M. Shin, I. S. Lee, D. Cho, Y. K. Chung, *Inorg. Chem.*, 2003, **42**, 7722; (*c*) B, Liu, C. Ren, Y. Wang, L. Hou, R. Liu, Q. Shi, *Sci China Chem.*, 2012, **55**, 341; (*d*) T. -F. Liu, J. Lü, R. Cao, *CrystEngComm*, 2010, **12**, 660.

(6) (*a*) B. Liu, R. Zhao, K. Yue, J. Shi, Y. Yu, Y. Wang, *Dalton Trans.*, 2013, **42**, 13990; (*b*) F. Gándara, M. E. Medina, N. Snejko, E. Gutiérrez-Puebla, D. M. Proserpio, M. Monge, *CrystEngComm*, 2010, **12**, 711; (*c*) S.-R. Zheng, Q.-Y. Yang, R. Yang, M. Pan, R. Cao, C.-Y. Su, *Cryst. Growth Des.*, 2009, **9**, 2341.

(7) (*a*) H. R. Khavasi, B. Mir Mohammad Sadegh, *Inorg. Chem.*, 2010, **49**, 5356; (*b*) B. Liu, L.-Y. Pang, L. Hou, Y.-Y. Wang, Y. Zhang, Q.-Z. Shi, *CrystEngComm*, 2012, **14**, 6246; (*c*) P.-X. Yin, J. Zhang, Y.-Y. Qin, J.-K. Cheng, Z.-J. Li, Y.-G. Yao, *CrystEngComm*, 2011, **13**, 3536; (*d*) B. Liu, H. Miao, L.-Y. Pang, L. Hou, Y.-Y. Wang, Q.-Z. Shi, *CrystEngComm*, 2012, **14**, 2954; (*e*) C.-P. Li, M. Du, *Chem. Commun.*, 2011, **47**, 5958; (*f*) L.-S. Long, *CrystEngComm*, 2010, **12**, 1354.

(8) (*a*) D. N. Dybtsev, H. Chun, K. Kim, *Angew. Chem. Int. Ed.,* 2004, **43**, 5033; (*b*) B. Liu, R. Zhao, G. Yang, L. Hou, Y.-Y. Wang, Q.-Z. Shi, *CrystEngComm,* 2013, **15**, 2057; (*c*) L.-F. Ma, L.-Y. Wang, X. K. Huo, Y.-Y. Wang, Y.-T. Fan, J.-G. Wang, S.-H. Chen, *Cryst. Growth Des.*, 2008, **8**, 620.

(9) (*a*) H. K. Chae, D. Y. Siberio-Pérez, J. Kim, Y. Go, M. Eddaoudi, A. J. Matzger, M. O,Keeffe, O. M. Yaghi, *Nature*, 2001, **427**, 523; (*b*) O. M. Yaghi, M. O'Keeffe,

N. W. Ockwig, H. K. Chae, M. Eddaoudi, J. Kim, *Nature*, 2003, **423**, 705; (*c*) G. Q. Kong, C. D. Wu, *Cryst. Growth Des.*, 2010, **10**, 4590; (*d*) B. Liu, Y. Li, L. Hou, G. Yang, Y.-Y. Wang, Q.-Z. Shi, *J. Mater. Chem. A*, 2013, **1**, 6535.

(10) (*a*) Q. Yang, X. Chen, Z. Chen, Y. Hao, Y. Li, Q. Lu, H. Zheng, *Chem. Commun.*, 2012, **48**, 10016; (*b*) J.-W. Lin, P. Thanasekaran, J.-S. Chang, J.-Y. Wu, L.-L. Lai, K.-L. Lu, *CrystEngComm*, 2013, **15**, 9798; (*c*) A. M. Plonka, D. Banerjee, W. R. Woerner, Z. Zhang, J. Li, J. B. Parise, *Chem. Commun.*, 2013, **49**, 7055; (*d*) H. Zhou, G.-X. Liu, X.-F. Wang, Y. Wang, *CrystEngComm*, 2013, **15**, 1377.

(11) (*a*) L. Du, Z. Lu, K. Zheng, J. Wang, X. Zheng, Y. Pan, X. You, J. Bai, *J. Am. Chem. Soc.*, 2013, **135**, 562; (*b*) B. Liu, L. Hou, Y.-Y. Wang, H. Miao, L. Bao, Q.-Z. Shi, *Dalton Trans.*, 2012, **41**, 3209; (*c*) J. Jia, X. Lin, C. Wilson, A. J. Blake, N. R. Champness, P. Hubberstey, G. Walker, E. J. Cussen, M, Schröder, *Chem. Commun.*, 2007, 840; (*d*) B. Liu, L. Wei, N. Li, W.-P. Wu, H. Miao, Y.-Y. Wang, Q.-Z. Shi, *Cryst. Growth Des.*, 2014, **14**, 1110; (*e*) Y.-S. Wei, K.-J. Chen, P.-Q. Liao, B.-Y. Zhu, R.-B. Lin, H.-L. Zhou, B.-Y. Wang, W. Xue, J.-P. Zhang, X.-M. Chen, *Chem. Sci.*, 2013, **4**, 1539.

(12) (*a*) G. M. Sheldrick, *Acta. Crystallogr., Sect. A*, 1990, **46**, 467; (*b*) G. M. Sheldrick, *SHELXS; University of Göttingen: Germany,* 1997; (*c*) W. Madison, *Bruker APEX2 Software, V2.0-1; Bruker AXS Inc.: USA,* 2005; (*d*) G. M. Sheldrick, *SADABS, Program for Empirical Absorption Correction of Area Detector Data; University of Göttingen: Germany,* 1997; (*e*) G. M. Sheldrick, *SHELXL, Program for the Refinement of Crystal Structures; University Göttingen: Germany,* 1997; (*f*)

A. L. Spek, *J. Appl. Crystallogr.* 2003, **36**, 7.

(13) (*a*) J.-Y. Zhang, X.-B. Li, K. Wang, Y. Ma, A.-L. Cheng, E.-Q. Gao, *Dalton Trans.*, 2012, **41**, 12192; (*b*) H. J. Park, M. P. Suh, *CrystEngComm*, 2012, **14**, 2748; (*c*) D. Deng, L. Liu, B.-M. Ji, G. Yin, C. Du, *Cryst. Growth Des.*, 2012, **12**, 5338; (*d*) M. Yang, F. Jiang, Q. Chen, Y. Zhou, R. Feng, K. Xiong, M. Hong, *CrystEngComm*, 2011, **13**, 3971.

(14) (*a*) S.-J. Liu, L. Xue, T.-L. Hu, X.-H. Bu, *Dalton Trans.*, 2012, **41**, 6813; (b) J. Cui, Y. Li, Z. Guo, H. Zheng, *Cryst. Growth Des.*, 2012, **12**, 3610; (*c*) H. L. Wang, D. P. Zhang, D. F. Sun, Y. T. Chen, L. F. Zhang, L. J. Tian, J. Z. Jiang, Z. H. Ni, *Cryst. Growth Des*., 2009, **9**, 5273; (*d*) F. P. Huang, J. L. Tian, W. Gu, X. Liu, S. P. Yan, D. Z. Liao, P. Cheng, *Cryst. Growth Des.*, 2010, **10**, 1145.

(15) R. Singh, M. Ahmad, P. K. Bharadwaj, *Cryst. Growth Des.*, 2012, **12**, 5028.

(16) L.-F. Ma, L.-Y. Wang, Y.-Y. Wang, M. Du, J.-G. Wang, *CrystEngComm*, 2009, **11**, 109.

(17) (*a*) H. He, F. Dai, D. Sun, *Dalton Trans.*, 2009, 763; (*b*) D. Sun, Z.-H. Yan, V. A. Blatov, L. Wang, D.-F. Sun, *Cryst. Growth Des.*, 2013, **13**, 1277.

(18) L.-F. Ma, L.-Y. Wang, Y.-Y. Wang, S. R. Batten, J.-G. Wang, *Inorg Chem.*, 2009, **48**, 915.

(19) (*a*) D. S. Li, J. Zhao, Y. P. Wu, B. Liu, L. Bai, K. Zou, M. Du, *Inorg Chem.*, 2013, **52**, 8096; (*b*) B. Liu, L. Pang, G. Yang, L. Cui, Y.-Y. Wang, Q. Shi, *CrystEngComm,* 2013, **15**, 5205.

(20) L. Schlapbach, A. Züttel, *Nature*, 2001, **414**, 353.

(21) (*a*) B. Bhattacharya, R. Haldar, R. Dey, T. K. Maji, D. Ghoshal, *Dalton Trans.*, 2014, **43**, 2272; (*b*) T. İslamoğlu, M. G. Rabbani, H. M. El-Kaderi, *J. Mater. Chem. A*, 2013, **1**, 10259; (*c*) Z. Lu, L. Du, B. Zheng, J. Bai, M. Zhang, R. Yun, *CrystEngComm*, 2013, **15**, 9348.

(22) M. D. Allendorf, C. A. Bauer, R. K. Bhakta, R. J. T. Houk, *Chem. Soc. Rev.*, 2009, **38**, 1330.

(23) (*a*) P. Cui, Z. Chen, D. L. Gao, B. Zhao, W. Shi, P. Cheng, *Cryst. Growth Des.* 2010, **10**, 4370; (*b*) Y. Q. Sun, J. Zhang, Y. M. Chen, G. Y. Yang, A*ngew. Chem. Int. Ed.*, 2005, **44**, 5841; (*c*) G. Q. Kong, C. D. Wu, *Cryst. Growth Des.*, 2010, **10**, 4590.

(24) (*a*) L. Wen, Y. Li, Z. Lu, J. Lin, C. Duan, Q. Meng, *Cryst. Growth Des.*, 2006, **6**, 530; (*b*) J.-G. Lin, S.-Q. Zang, Z.-F. Tian, Y.-Z. Li, Y.-Y. Xu, H.-Z. Zhu, Q.-J. Meng, *CrystEngComm*, 2007, **9**, 915; (*c*) L.-F. Ma, L.-Y. Wang, J.-L. Hu, Y.-Y. Wang, G.-P. Yang, *Cryst. Growth Des.*, 2009, **9**, 5341.

(25) H.-Y. Liu, H. Wu, J.-F. Ma, Y.-Y. Liu, B. Liu, J. Yang, *Cryst. Growth Des.*, 2010, **10**, 4795.

Captions to Figures

Figure 1. View of (a) the coordination environment of Co(II), symmetry code: i 3-x, -y, 1-z, ii -1+x, 1+y, z, iii 1+x, y, -1+z; (b) the 2D layer; (c) the 4^4 topology net in **1**. Co(II) ions are taken as nodes; L^{2-} anions are substituted by sticks.

Figure 2. View of (a) the coordination environment of Co(II), symmetry code: i 1-x, 3-y, 2-z, ii 2-x, 1-y, 1-z; (b) the 2D layer; (c) the 4^4 topology network in **2**. Co(II) ions are taken as nodes, L^{2-} anions are substituted by sticks.

Figure 3. View of (a) the coordination environment of Co(II), symmetry code: i -0.5+x, -0.5+y, z, ii x, -y, -0.5+z, iii 1.5-x, -0.5-y, -z, iv 1-x, -1+y, 0.5-z, v 1-x, -1-y, -z; (b) 3D framework from trinuclear Co(II) clusters linked by L^{2-} anions; (c) the linkage of the Co3 clusters with ten adjacent cores; (d) schematic view of the 3D network topology. The gray spheres represent the trinuclear Co(II) units, and the green spheres represent the L^{2-} anion.

Figure 4. View of (a) the coordination environment of Co(II), symmetry code: i x, 0.5-y, 0.5+z, ii 2-x, -y, 2-z, iii -1+x, y, z, iv 2-x, 1-y, 2-z, v 1-x, 1-y, 2-z, vi 1-x, -0.5+y, 1.5-z; (b) 3D framework from pentanuclear Co(II) clusters linked by L^{2-} anions; (c) the linkage of the Co5 clusters with twelve adjacent cores; (d) schematic view of the 3D network topology; (e) space-filling model of **4** along c axis showing the large 1D channels, the guest solvent molecules are omitted for clarity.

Figure 5. View of (a) the coordination environment of Mn(II), symmetry code: i -x, 2-y, 1-z, ii 1+x, -1+y, z, iii x, y, -1+z; (b) the 2D layer; (c) the 4^4 topology network in **5**. Mn(II) ions are taken as nodes, L^{2-} anions are substituted by sticks.

Figure 6. View of (a) the coordination environment of Zn(II), symmetry code: i -x, y, 0.5-z, ii 1-x, y, 1.5-z, iii x, -y, -0.5+z, iv 1-x, -y, 2-z; (b) the DNA-like chain; (c) the 2D layer in **6**; (d) 3D framework from Zn(II) chains linked by L^{2-} anions.

Figure 7. Temperature dependence of $\chi_M T$ and χ_M versus T of **1**−**5**. Inset: temperature dependence of χ_M^{-1}, (a) **1**, (b) **2**, (c) **3**, (d) **4**, and (e) **5**.

Figure 8. Gas sorption isotherms of **4**, (a) N_2, 77 K and CO_2 , 195 K; (b) H_2, 77 K.

Figure 9. Fluorescent emission spectra of free ligand H_2L and **6** in the solid state at

room temperature.

Figures

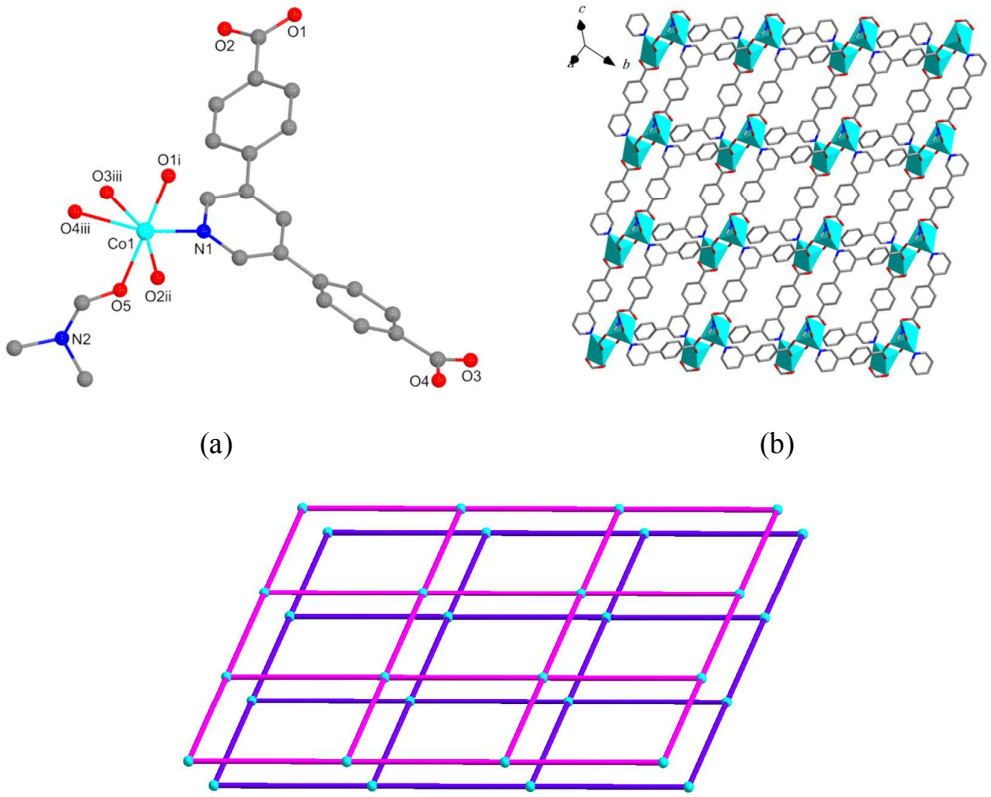

Figure 1

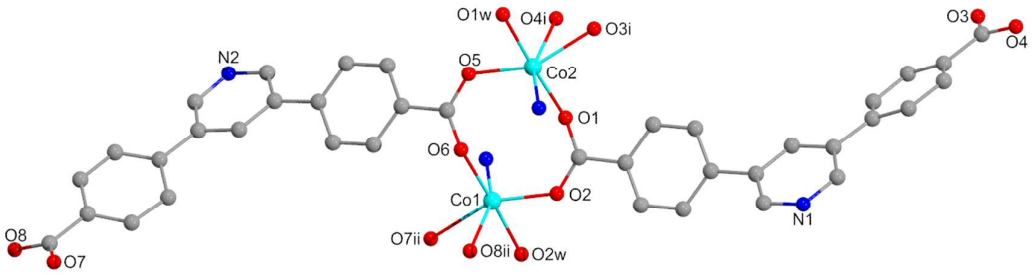

(a)

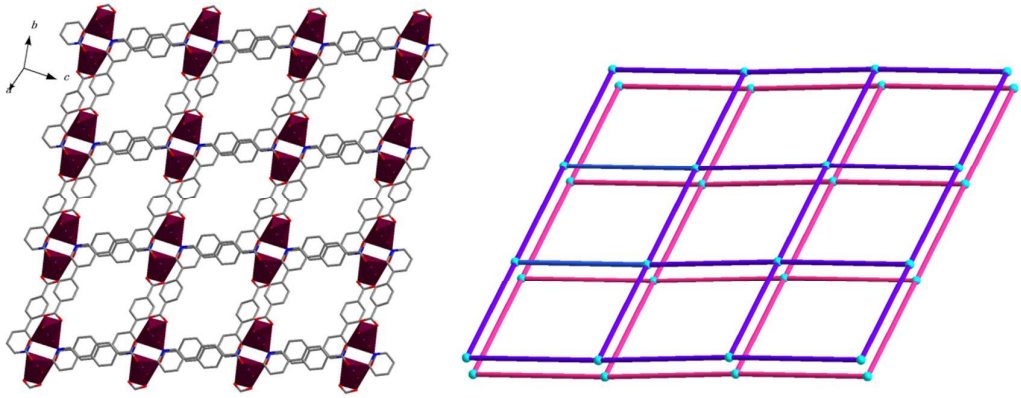

(b) (c)

Figure 2

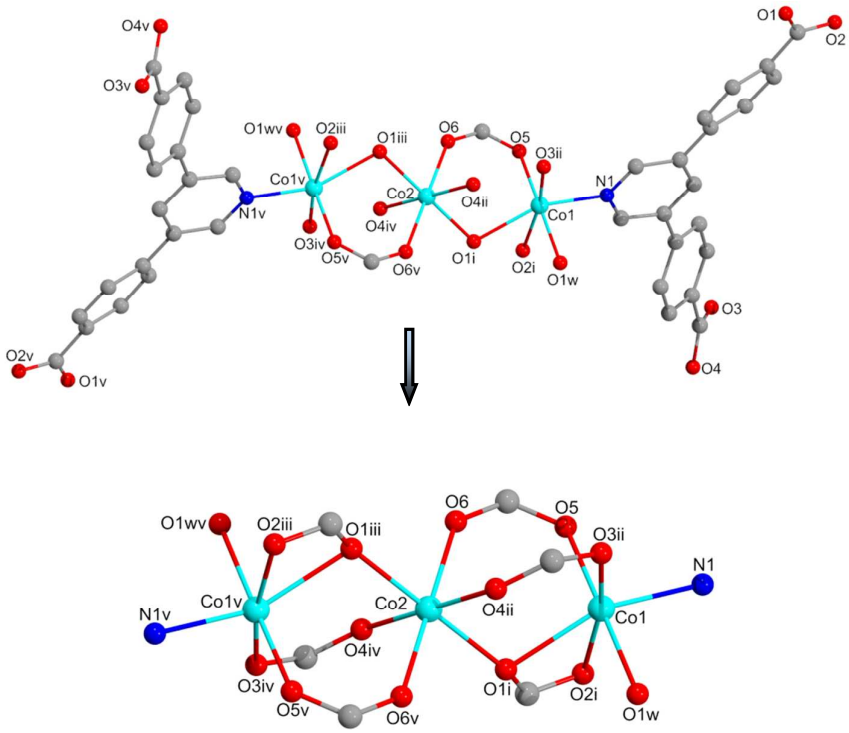

(a)

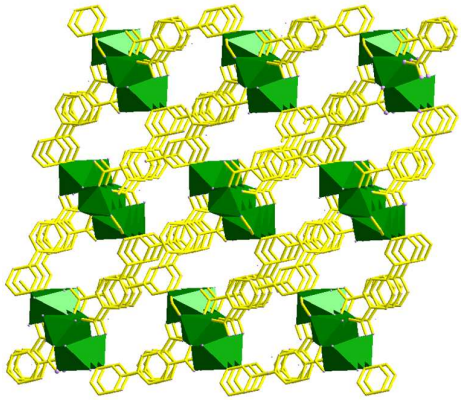

(b)

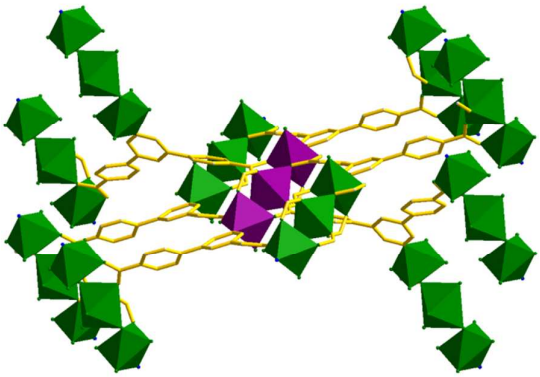

(c)

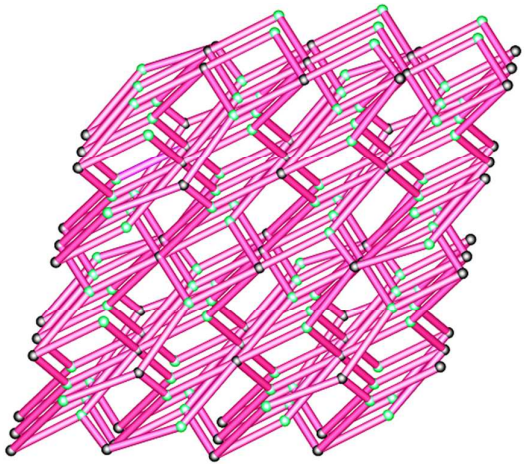

(d)

Figure 3

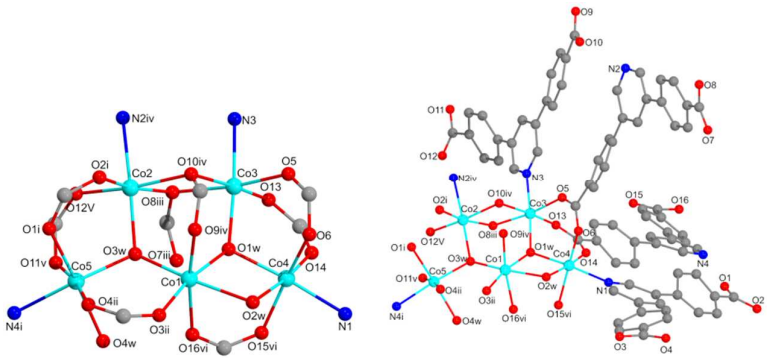

(a)

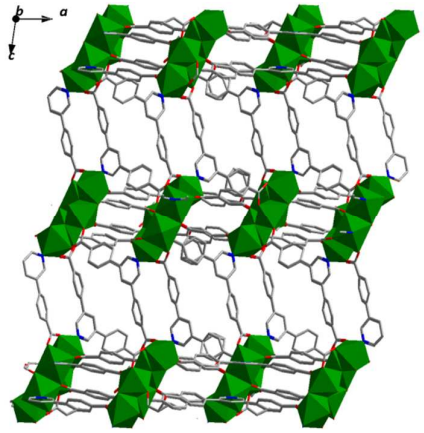

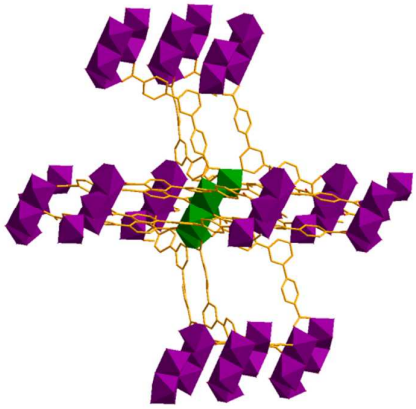

(b) (c)

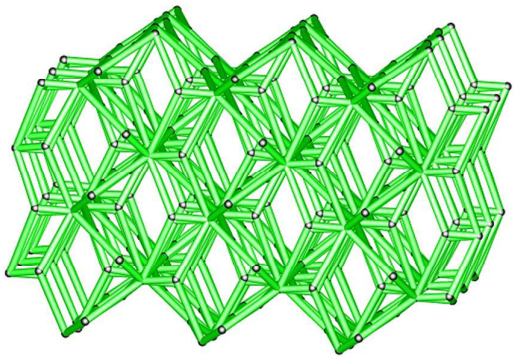

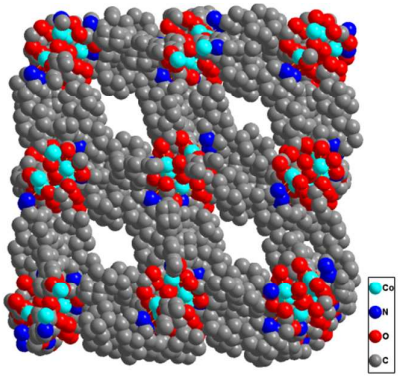

(d) (e)

Figure 4

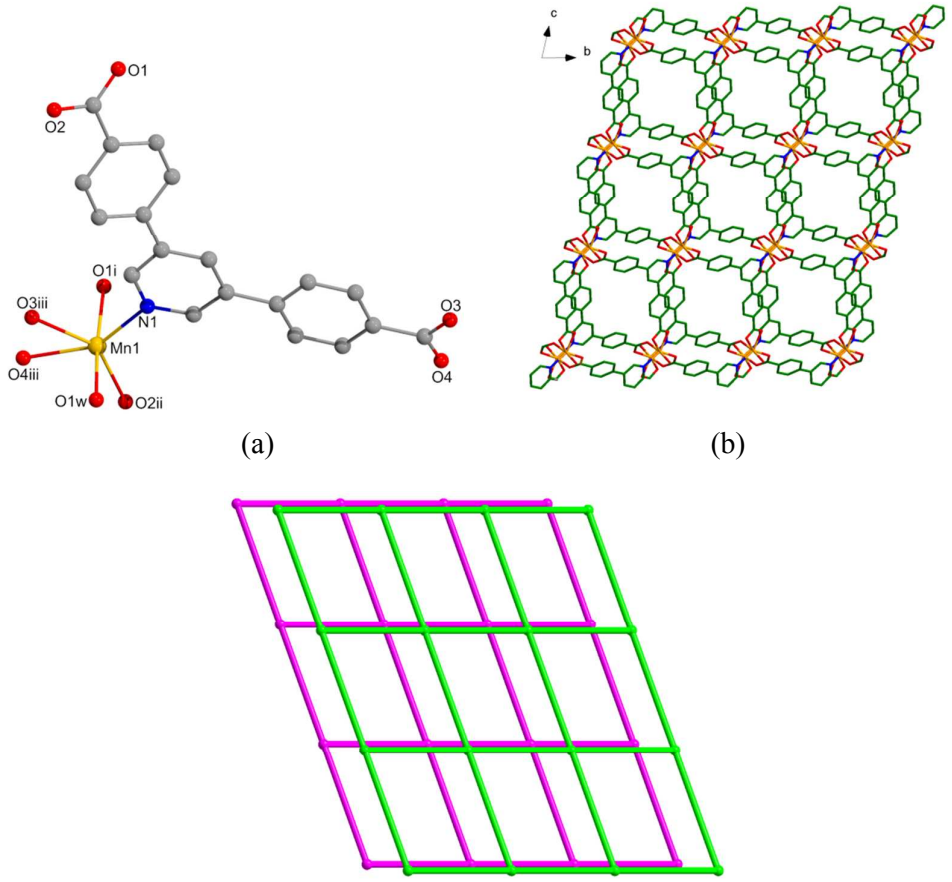

(a) (b)

(c)

Figure 5

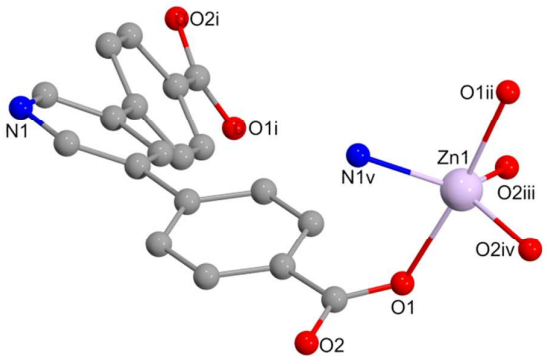

(a)

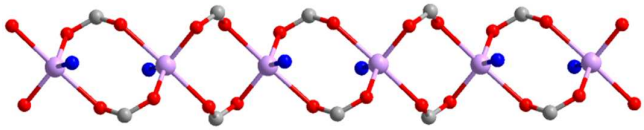

(b)

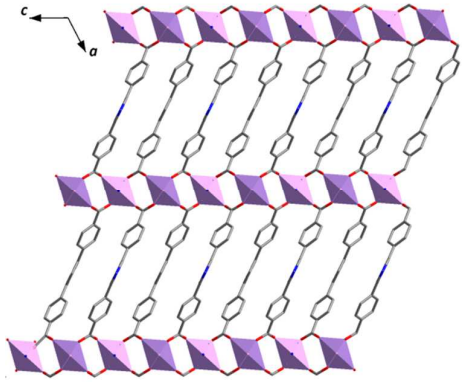

(c)

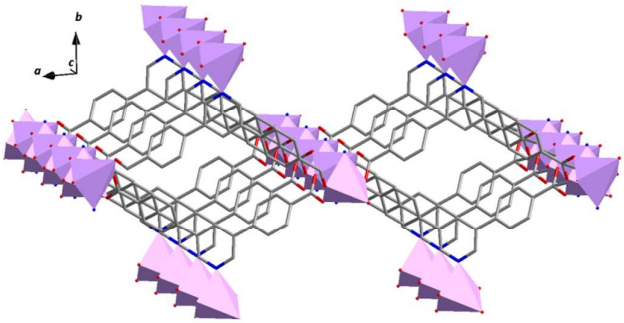

(d)

Figure 6

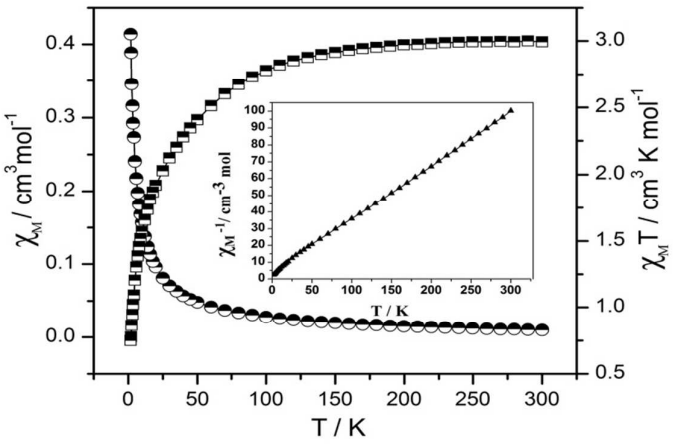

(a)

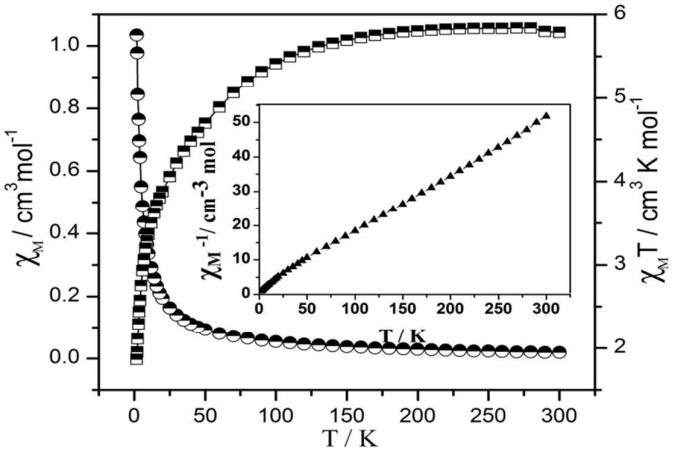

(b)

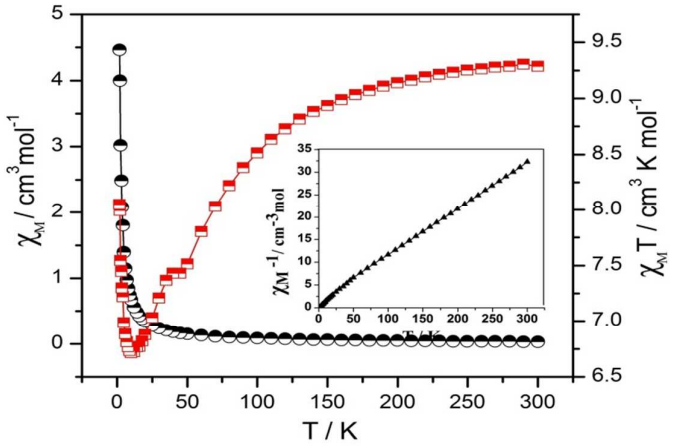

(c)

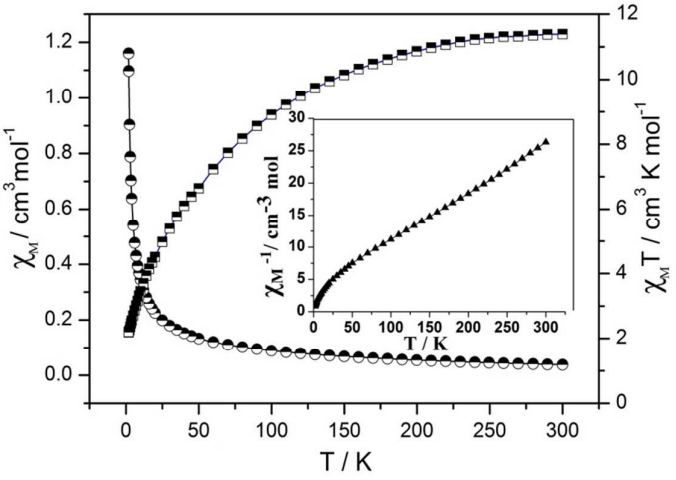

(d)

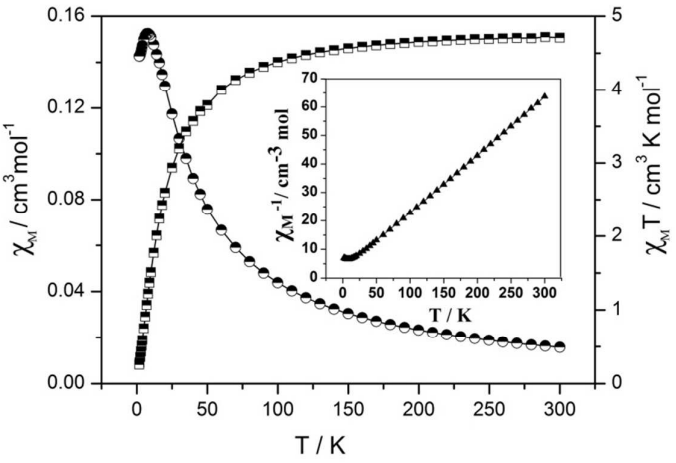

(e)

Figure 7

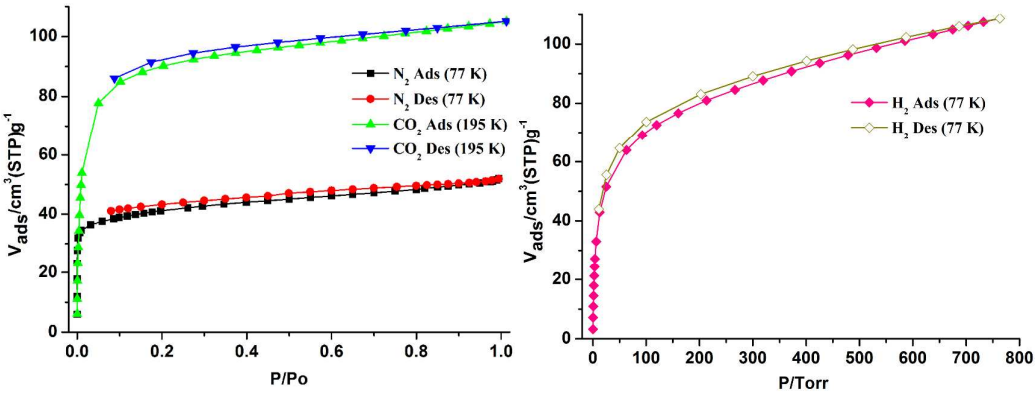

(a) (b)

Figure 8

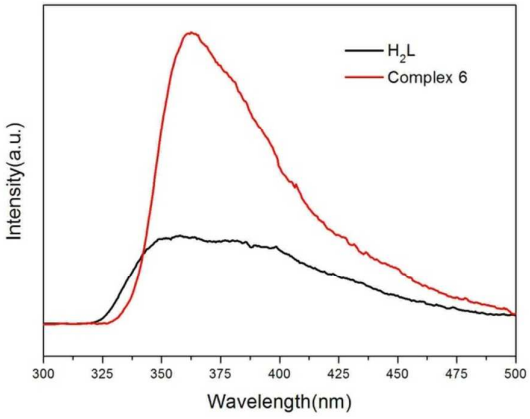

Figure 9

Table 1. Crystallographic Data and Structure Refinements for Complexes **1**−**6**

Complexes	**1**	**2**	**3**	**4**	**5**	**6**
Formula	$C_{22}H_{18}N_2O_5Co$	$C_{22}H_{20}N_2O_6Co$	$C_{40}H_{28}N_2O_{14}Co_3$	$C_{77.5}H_{55.5}N_{4.5}O_{21.5}Co_5$	$C_{22}H_{20}N_2O_6Mn$	$C_{22}H_{18}N_2O_5Zn$
Mr	449.31	467.32	937.47	1688.48	463.35	455.78
Crystal system	triclinic	triclinic	monoclinic	monoclinic	triclinic	monoclinic
Space group	*P*-1	*P*-1	*C2/c*	$P2_1/c$	*P*-1	*C2/c*
a (Å)	10.469(10)	9.690(3)	22.476(5)	18.7481(18)	9.6769(17)	17.343(17)
b (Å)	10.611(11)	11.998(4)	7.7060(18)	20.0714(19)	10.0627(18)	15.231(15)
c (Å)	11.429(11)	19.891(7)	22.255(5)	32.864(3)	12.108(2)	8.426(12)
α (°)	89.177(14)	96.548(4)	90	90	72.146(2)	90
β (°)	65.827(13)	99.122(4)	102.056(11)	98.5350(10)	66.911(2)	117.09(2)
γ (°)	66.661(13)	113.712(4)	90	90	74.995(2)	90
V(Å3)	1046.8(18)	2049.6(12)	3769.7(15)	12230	1019.3(3)	1982(4)
Z	2	2	4	2	2	4
Dcalcd(g·cm-3)	1.425	1.383	1.652	0.917	1.510	1.282
μ(mm-1)	0.855	0.880	1.380	0.712	0.691	1.277
GOF	1.041	1.129	1.063	1.093	1.122	1.152
R_1 [I>2σ(I)]a	0.0640	0.0510	0.0288	0.0640	0.0600	0.0366
wR_2 [I>2σ(I)]b	0.1829	0.1576	0.0798	0.1975	0.1709	0.1070
R_1[a] (all data)	0.0727	0.0571	0.0315	0.1164	0.0796	0.0404
wR_2[b] (all data)	0.1916	0.1660	0.0817	0.2584	0.2030	0.1088
R_{int}	0.0282	0.0309	0.0213	0.0798	0.0326	0.0296

[a] $R_1 = \sum\big|\,|F_o|-|F_c|\,\big| / \sum|F_o|$. [b] $wR_2 = \big|\sum w(|F_o|^2-|F_c|^2)\big| / \sum\big|w(F_o^2)^2\big|^{1/2}$

Graphic content (TOC)

Using a rigid ligand, pyridine-3,5-bis(phenyl-4-carboxylic) acid, six new coordination polymers have been synthesized and characterized, the magnetic, photoluminescence and the gases adsorption properties have been studied.